Matter and Radiation at Extremes | RESEARCH ARTICLE | scitation.org/journal/mre

Crystallography of low Z material at ultrahigh pressure: Case study on solid hydrogen

Cite as: Matter Radiat. Extremes 5, 038401 (2020); doi: 10.1063/5.0003288
Submitted: 31 January 2020 • Accepted: 15 March 2020 •
Published Online: 28 April 2020

Cheng Ji,[1,2] Bing Li,[1,3] Wenjun Liu,[4] Jesse S. Smith,[5] Alexander Björling,[6] Arnab Majumdar,[7] Wei Luo,[7] Rajeev Ahuja,[7] Jinfu Shu,[1] Junyue Wang,[1] Stanislav Sinogeikin,[2,a)] Yue Meng,[5] Vitali B. Prakapenka,[8] Eran Greenberg,[8,b)] Ruqing Xu,[4] Xianrong Huang,[4] Yang Ding,[1] Alexander Soldatov,[1,9] Wenge Yang,[1] Guoyin Shen,[5] Wendy L. Mao,[10,11] and Ho-Kwang Mao[1,c)]

AFFILIATIONS

[1] Center for High Pressure Science and Technology Advanced Research, Beijing 100094, China
[2] High Pressure Collaborative Access Team, Geophysical Laboratory, Carnegie Institution of Washington, Argonne, Illinois 60439, USA
[3] Center for the Study of Matter at Extreme Conditions and Department of Mechanical and Materials Engineering, Florida International University, Miami, Florida 33199, USA
[4] Advanced Photon Source, Argonne National Laboratory, Lemont, Illinois 60439, USA
[5] HPCAT, X-Ray Science Division, Argonne National Laboratory, Lemont, Illinois 60439, USA
[6] MAX IV Laboratory, Lund University, 22100 Lund, Sweden
[7] Condensed Matter Theory Group, Materials Theory Division, Department of Physics and Astronomy, Uppsala University, Uppsala S-75120, Sweden
[8] Center for Advanced Radiation Sources, University of Chicago, Chicago, Illinois 60637, USA
[9] Department of Engineering Sciences and Mathematics, Luleå University of Technology, 97187 Luleå, Sweden
[10] Department of Geological Sciences, Stanford University, Stanford, California 94305, USA
[11] Stanford Institute for Materials and Energy Sciences, SLAC National Accelerator Laboratory, Menlo Park, California 94025, USA

Note: This paper is part of the Special Issue on High Pressure Science
[a)] **Present address:** DAC Tools LLC, Naperville, Illinois 60565, USA.
[b)] **Present address:** Applied Physics Department, Soreq Nuclear Research Center (NRC), Yavne 81800, Israel.
[c)] **Author to whom correspondence should be addressed:** maohk@hpstar.ac.cn

ABSTRACT

Diamond anvil cell techniques have been improved to allow access to the multimegabar ultrahigh-pressure region for exploring novel phenomena in condensed matter. However, the only way to determine crystal structures of materials above 100 GPa, namely, X-ray diffraction (XRD), especially for low *Z* materials, remains nontrivial in the ultrahigh-pressure region, even with the availability of brilliant synchrotron X-ray sources. In this work, we perform a systematic study, choosing hydrogen (the lowest X-ray scatterer) as the subject, to understand how to better perform XRD measurements of low *Z* materials at multimegabar pressures. The techniques that we have developed have been proved to be effective in measuring the crystal structure of solid hydrogen up to 254 GPa at room temperature [C. Ji *et al.*, Nature **573**, 558–562 (2019)]. We present our discoveries and experiences with regard to several aspects of this work, namely, diamond anvil selection, sample configuration for ultrahigh-pressure XRD studies, XRD diagnostics for low *Z* materials, and related issues in data interpretation and pressure calibration. We believe that these methods can be readily extended to other low *Z* materials and can pave the way for studying the crystal structure of hydrogen at higher pressures, eventually testing structural models of metallic hydrogen.

I. INTRODUCTION

Ultrahigh pressure compression, especially in the multimegabar region, can achieve energy densities comparable to those associated with bonding, and so significant changes in the electrical state, chemical bonding, and packing of condensed matter can be expected, resulting in novel structural, chemical, electronic, or magnetic

properties.[1] For instance, at pressures above 1 Mbar, sodium turns from a metal to an insulator,[2] diatomic nitrogen (N_2) with a strong triple bond transforms into single-bonded extended structures,[3–6] and LaH_{10} is formed and exhibits near-room-temperature superconductivity.[7,8] These exciting discoveries continue to inspire research into the properties of matter in the very high-pressure region. In particular, recent developments in theoretical methods have allowed more reliable predictions of crystal structures under high pressure,[9–11] providing guidance in the search for materials with advanced properties, with H_3S (Ref. 12) and LaH_{10} (Refs. 7 and 8) being two prominent examples. Crystal structure is currently the main bridge connecting theoretical predictions and high-pressure experiments, and it provides the most fundamental information for understanding a material. However, even though pressures up to 400 GPa can be realized using a conventional diamond anvil cell (DAC),[13] and higher pressures have reportedly been achieved using novel DAC methods,[14–16] measurements of crystal structures of material at ultrahigh pressures remain challenging owing to the extremely small sample volumes of the order of picoliters to femtoliters (the anvil culet size has to be small to achieve ultrahigh pressures) and the complications associated with the DAC sample environment (thick diamond windows, confining materials with strong diffraction, etc.).

Synchrotron X-ray diffraction (XRD) is currently the only option for determining the crystal structure of a material above 100 GPa. However, such measurements are nontrivial at ultrahigh pressures. Even though the high-pressure synchrotron XRD technique itself has being evolving, with brighter X-ray sources, smaller focus areas, and better detectors (larger area, higher quantum efficiency, and lower background), etc., some essential problems remain. First, it is difficult to avoid strong scattering from the diamond anvils (Compton scattering) and the gasket materials that surround the tiny DAC sample. These background signals overwhelm sample signals when the sample is a low Z material (a weak X-ray scatterer). Second, even though the quasi-hydrostatic condition is desirable for providing an ideal comparison with theory, studies using the best hydrostatic pressure medium, namely, helium (He),[17] at ultrahigh pressures are difficult. This is due to the fact that He is highly diffusive and tends to induce premature failures of diamond anvils. Third, pressure calibration at very high pressures is not straightforward, owing to the lack of consensus regarding a single best caliber at ultrahigh pressures. Hydrogen is a perfect candidate for investigating the above problems. First, it is the weakest X-ray scatterer, for which successful XRD techniques would provide guidance for studying all other materials, especially low Z materials. Second, understanding how to confine hydrogen samples that are suitable for effective XRD measurements at ultrahigh pressures will guide experiments with He as pressure medium, since, like He, hydrogen is highly diffusive. Third, vibrational spectroscopy and XRD of hydrogen, as well as XRD of other pressure markers, can be measured together to help understand pressure calibration at very high pressures. In addition, studying XRD of high-pressure phases of hydrogen provides important information that is helpful in understanding basic questions in condensed matter physics, such as how does hydrogen evolve into the predicted metal and how to treat quantum motion as well as many–body interactions in theoretical calculations.

A rich phase diagram of solid hydrogen has been observed, namely, phase I,[18] phase II,[19] phase II′ (deuterium),[20] phase III,[21] phase IV,[22,23] phase IV′,[24] and phase V.[25] Most of these phases were discovered and investigated by spectroscopic methods, namely, Raman[18,22,25–29] and infrared[18,26,28–33] spectrometry. Through theoretical calculations, especially first-principles crystal structure prediction methods,[34–38] crystal structural models were picked up by their consistency with the spectroscopic results. The number of hydrogen XRD studies is very limited, however, owing to the significant experimental challenges, which leaves only phase I as being uniquely determined to have a hexagonal closed packed (hcp) structure.[18] One key to the previous success of XRD measurements is the preservation of a sizable single crystal of hydrogen at high pressure. By performing single-crystal XRD (SXRD) measurements, a in-house diffractometer was able to work at 5.5 GPa.[39] Increasing pressure defragments crystallites, and a much brighter synchrotron X-ray source is required to resolve XRD signals.[40] At pressures above 100 GPa, a novel approach of preserving a single crystal of hydrogen using helium as the pressure medium was adopted, which allowed the pressure limit to be extended to 120 GPa at room temperature (RT).[41] There have also been reports of powder XRD measurements at low temperature that probed phases II and III up to 190 GPa at 100 K.[42,43] In our study, the target was the recently discovered phase IV,[22] which is the first phase of hydrogen to be found to exhibit two fundamental vibrons[22] and requires the compression of hydrogen above 220 GPa at RT (hydrogen is more diffusive and damaging to diamond anvils at RT than at low temperature). Upgrades to both sample preparation and diagnostic techniques are required to overcome the daunting experimental challenges involved.[44]

In this study, we performed a systematic investigation to understand how to confine hydrogen and measure its XRD properties under these challenging conditions. We present our findings on the axial pressure distribution, selection of anvils, sample preparation, XRD measurement techniques [nano beam and multichannel collimator (MCC)], and data interpretation, as well as on pressure calibration at ultrahigh pressures. Our work will provide guidance for ultrahigh-pressure XRD studies of not only solid hydrogen, but also all materials, especially low Z materials.

II. EXPERIMENTAL

Two types of gases were used as starting materials. Premixed normal H_2 and He gas of 99.9% purity with 1:4 volume ratio was chosen for growing isolated single crystals of solid hydrogen in an He environment (H_2–He samples). Normal H_2 gas with purity of 99.99% (pure-H_2 samples) was used for experiments with a nano beam and MCC. All gases were purchased from Airgas Inc. Symmetric DACs were used to generate high pressure. Force was delivered by screws with Belleville washers to avoid any piping connection (in the case when a membrane was used), since rotation of DACs would be required during XRD data collection. Beveled diamond anvils of Boehler–Almax design[45] with culet size ranging from 150 μm down to 20 μm were used, with 50 μm (H_2–He samples) and 30 μm (pure-H_2 samples) being the most used sizes. All anvils were beveled from 300 μm with an 8.5° bevel angle. For H_2–He samples, holes ~30 μm in diameter were drilled in pre-indented (30 GPa) tungsten (W) or rhenium (Re) gaskets as sample chambers. For pure-H_2 samples, composite gaskets with Re framework and magnesium oxide (MgO) + epoxy or cubic boron nitride (cBN) + epoxy inserts were used. All sample chambers were fabricated using the laser microfabrication system at the High Pressure Collaborative Access Team (HPCAT) of the Carnegie Institution of Washington.[46] For the majority of H_2–He

samples, thin gold (Au) chips were loaded into the sample chamber as pressure markers. The (111) reflection of Au standard was used to calculate pressure.[47] Ruby was used as pressure marker[48] for the sample with 150 μm culet size. All samples were loaded by sealing compressed hydrogen at 0.16 GPa using gas loading systems at the Advanced Photon Source (APS) at Argonne National Laboratory (ANL), the Geophysical Laboratory of the Carnegie Institution of Washington, or the Center for High Pressure Science and Technology Advanced Research, Shanghai (HPSTAR). White beam X-ray topographic characterizations of diamond anvils were performed at beamline 1-BM of the APS. The topographic images were measured using a white beam with 1 s exposure and were recorded using X-ray films with 1 μm spatial resolution. The axial pressure distribution was measured using a confocal micro-Raman system at the APS. The measurements were performed using a 659.5 nm excitation laser, with backscattering geometry recorded using a charge coupled device (CCD) camera. The grating of the spectrometer used was 300 lines/mm, which yields a resolution of ~2.5 cm^{-1} at the frequency of the diamond Raman edge. Synchrotron XRD studies have been performed on multiple advanced synchrotron beamlines, including 34 IDE, 16 IDB, and 13 IDD at the APS, NanoMAX at MAX IV, BL15U1 at the Shanghai Synchrotron Radiation Facility (SSRF), and BL10XU at SPring8. The H_2–He samples were studied on 16 IDB with a 6×7 μm^2 focused monochromatic beam at 30 keV (using a Pilatus 1M or Mar165CCD detector), on 13 IDD with a 3×2 μm^2 focused monochromatic beam at 37 keV (Mar165CCD detector), and on BL15U1 with a 2×2 μm^2 focused monochromatic beam at 20 keV (Mar165CCD detector). Nano-diffraction experiments on pure-H_2 samples were performed on 34 IDE with a 300 nm focused monochromatic beam at 23–24 keV (Mar165CCD detector), on NanoMAX with a 50 nm focused monochromatic beam at 20 keV (Pilatus 1M detector), and on BL10XU with a 1000×700 nm^2 focused monochromatic beam at 30 keV (R-AXIS IV++ image plate detector). All these beamlines use a Kirkpatrick–Baez mirror as the focusing device, except BL10XU, which uses a compound refractive lens.[49] Studies of pure-H_2 with a MCC were performed on 16 IDB with a 6×7 μm^2 or a 2×1 μm^2 focused monochromatic beam at 30 keV (Pilatus 1M detector). Dioptas[50] was used for data reduction. Fityk[51] was used to perform peak fitting to subtract the peak positions of the XRD peaks. EoSFit7-GUI[52] was used for fitting the equation of state (EOS). 2D XRD contrast imaging was analyzed using XDI.[53]

III. RESULTS AND DISCUSSION

In this section, we report our investigations in the following structured way. There are primarily three challenges in our experiments. The first is to confine hydrogen under ultrahigh pressure. To understand this problem, we began by studying the stress distribution in diamond anvils at very high pressures (Sec. III A). Following these results, we used topographic imaging to select appropriate diamond anvils for experiments (Sec. III B). The sample size was also noticed to have a critical effect on the final pressure in the case of a highly diffusive sample or pressure medium (Sec. III C). The second challenge is to make small samples suitable for XRD measurements. We utilized a composite gasket with light material inserts, and successfully addressed this problem (Sec. III D). The third challenge is to effectively investigate XRD of hydrogen above 200 GPa, as described in Sec. III E, where we discuss three types of measurement techniques, as well as tricks and pitfalls in data interpretation of XRD of low Z materials, and provide a comparison of the different methods. Finally, we discuss pressure calibration at ultrahigh pressure by comparing multiple pressure markers in Sec. III F.

A. Axial pressure distribution

Understanding the behavior of diamond anvils under extreme compression provides fundamental information for improving the performance of ultrahigh-pressure experiments. Even though diamond is the hardest material, it is subject to plastic deformation[54] and breaks unpredictably under ultrahigh pressure. The performance of diamond anvils varies depending on the geometry of their design and their natural quality. Understanding the pressure distribution of a diamond anvil under multimegabar pressures is crucial for developing techniques to achieve higher pressures and to establish criteria for selection of anvils. The pressure distribution of diamond anvils at the anvil–sample interface up to 400 GPa has been studied previously by combining nano-beam X-ray diffraction and X-ray absorption techniques.[13] Measurements under these conditions are of critical importance, since 400 GPa is considered to be the limiting pressure achievable using beveled diamond anvils. It is clear that the stress is strongly concentrated within the small beveled area and that the highest pressure is found at the center of the culet. However, there have been few experimental studies of the axial pressure distribution (the pressure distribution along the compression axis) under ultrahigh pressures. Here, we map the axial pressure distributions of diamond anvils with a hydrogen sample at 228 GPa using microfocus confocal Raman spectroscopy, as shown in Fig. 1. The stress is concentrated in the region close to the anvil–sample interface, where the sample is located. By sampling the pressure from the hydrogen sample to the interior of the diamond anvil along the laser path, which is also the compression axis, it is found that the pressure first increases slightly from 228 GPa to 238 GPa (35 μm away from the hydrogen) and then drops rapidly inside the anvil. The pressure at a depth of 110 μm away from hydrogen already drops to 20 GPa, less than 10% of the sample pressure [Fig. 1(d)]. Considering the depth of field of the system [Fig. 1(b)], the pressure drops to 10% of the maximum at a depth of 110 ± 80 μm. Based on the pressure distribution measurements, it can be conservatively estimated that the tip of the beveled culet area with a depth below 200 μm is the most critical portion of the diamond anvil and is subject to the majority of the stress (in the case of a 200 GPa sample). It should be noted here that the Raman spectrum measured at each depth is a convolution of signals from materials within the depth of focus, and a confocal Raman system with shallower depth of focus would be desirable for achieving higher accuracy in such measurements. We therefore paid particular attention to the quality in the tip region when we selected diamond anvils for experiments.

B. White beam topographic imaging of diamond anvils

Synchrotron white beam topography imaging characterization was utilized for selecting appropriate diamond anvils for ultrahigh-pressure experiments on hydrogen. As the most critical portion of a diamond anvil is at the very tip, anvils with high quality, at least in the highly stressed tip region, need to be reliably selected for ultrahigh-pressure experiments. White beam topographic imaging based on

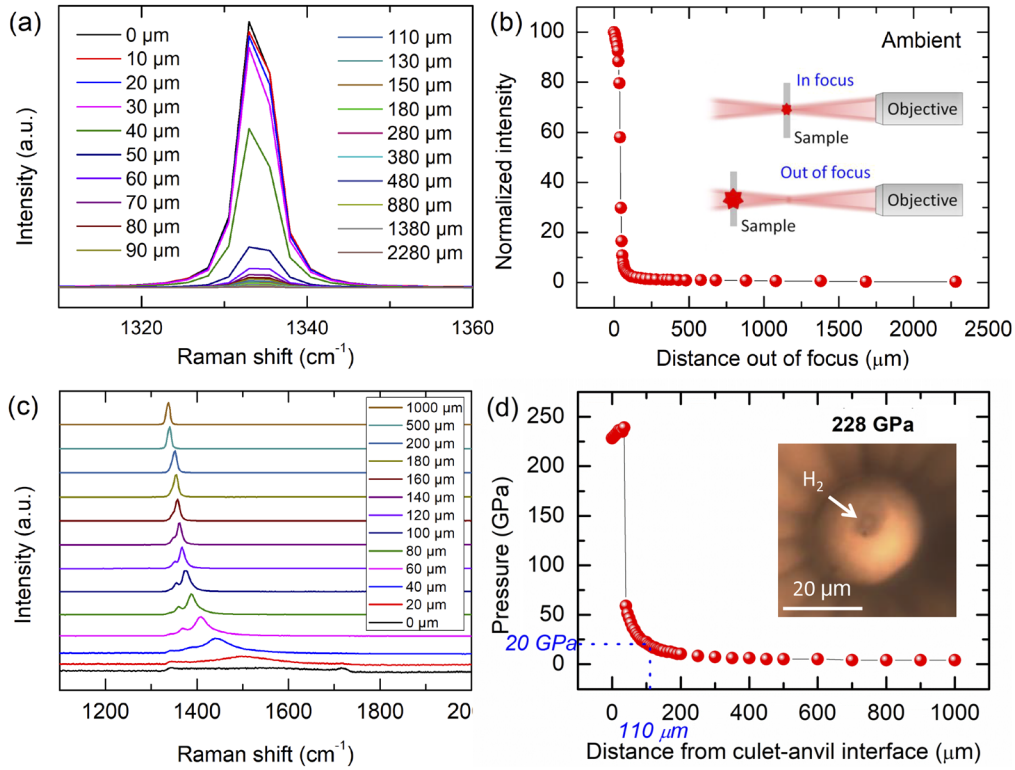

FIG. 1. Axial pressure distribution of a diamond anvil with a hydrogen sample at 228 GPa. (a) Raman spectra of the ambient diamond anvil measured with the laser beam in focus and out of focus at different distances. (b) Intensity of a diamond Raman phonon measured with the laser beam in focus and out of focus at different distances. The intensity drops to 50% at 40 μm. (c) Raman spectra of the diamond anvil measured with the laser beam in focus and out of focus with the sample at different depths. (d) Pressures at different depths away from the culet–anvil interface. The pressure increases slightly at shallow depths, with the intensity of the high-frequency diamond edge decreasing rapidly. At a depth of 40 μm, the high-frequency edge that corresponds to >200 GPa is hardly distinguishable. The hint of a high-frequency edge is due to convolution of the high-pressure signal with the finite depth of focus (80 μm). The pressure drops to ~20 GPa at 110 μm. The inset shows a microscope image of the sample with transmitted and reflected light.

transmission Laue diffraction is known to be a convenient tool for examining defects in diamond for high-performance X-ray optics applications.[55–57] While birefringence is commonly used for selecting anvils, topographic imaging methods are able to reveal almost all kinds of crystalline defects and strains in all directions. A detailed study of topographic imaging of diamond anvils has been reported,[58] which demonstrates that it is an efficient method to examine diamond anvils. We performed white beam topography imaging of diamond anvils to correlate the quality of the anvils with the pressures that were later achieved. The experimental setup is shown in Fig. 2(a). A diamond anvil is mounted (by amorphous Crystalbond adhesive) on a post holder that is connected to a goniometer. We measured the anvils with two orientations, one with the X-ray beam going along the compression axis and the other with the beam orthogonal to that axis. Figure 2(b) shows a developed film, where the darker spots are Laue reflections from a diamond anvil. We paid special attention to the results from the geometry where the X-ray beam was perpendicular to the compression axis. Such projections reveal the depth-dependent distribution of defects in the diamond anvil. Figure 2(c) shows an example of a damaged anvil, where cracks near the tip of the culet are revealed. Figures 2(d)–2(f) show examples of topographic images of anvils (ambient), with the corresponding microscopic images at their highest achieved pressures. The anvil with lowest quality at the tip experienced stronger plastic deformation at the highest pressure [Fig. 2(d)], while the other two anvils with higher quality survived higher pressures, showing no identifiable defects induced by plastic deformation [Figs. 2(e) and 2(f)]. A cross-hatched texture similar to that seen in Fig. 2(d) has also been reported in a previous study as a sign of plastic deformation.[59] The use of a transparent gasket (as will be detailed in Sec. III D) allows a clear observation of the development of such defects. Anvils that developed appearances of defects similar to that in Fig. 2(d) were not, in general, able to sustain pressures above 220 GPa and broke under increasing load. Anvils without texture, similar to those in Figs. 2(e) and 2(f), were in good conditions, but they broke owing to high doses of X-ray irradiation (we noticed that a high dose of X-ray photons can damage highly stressed diamond anvils in contact with hydrogen[44]). By endeavoring to distinguish high-quality anvils, we were able to achieve phase IV conditions in hydrogen with more confidence.

C. Sample configurations for quasi-hydrostatic ultrahigh-pressure experiments

To preserve high-quality crystallites of hydrogen for XRD measurements, as well as to accurately determine the EOS of

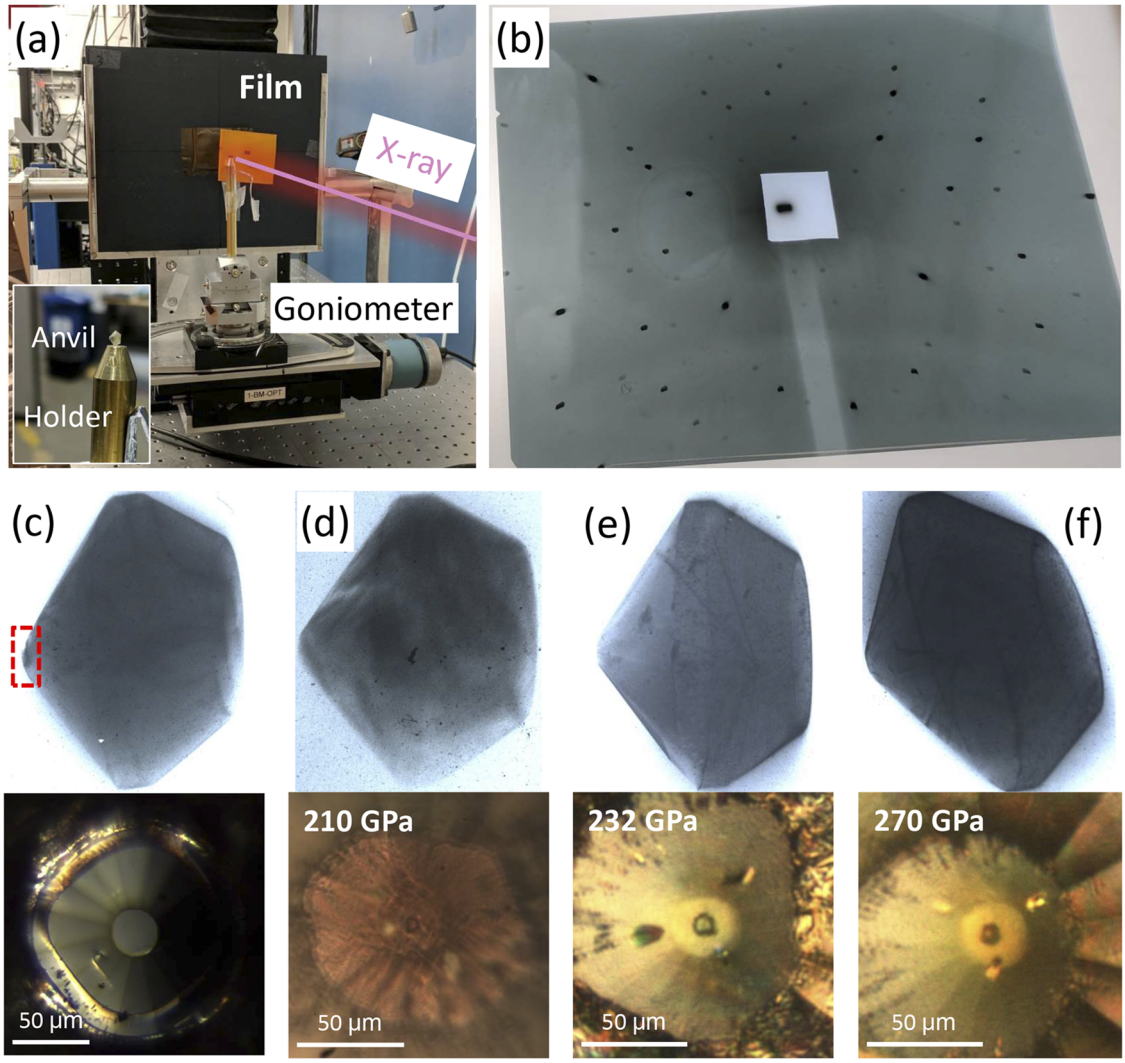

FIG. 2. Examination of diamond anvils by synchrotron white beam topographic imaging. (a) Experimental setups at beamline 1-BM of the APS at ANL. The inset shows the sample and sample holder. (b) Developed X-ray film with the recorded Laue pattern. (c)–(f) show topographic (top) and optical microscopic (bottom) images of selected anvils. (c) Example of a cracked diamond anvil, released from 200 GPa, where the red dashed box on the topographic image marks the cracked position while the corresponding microscopic image shows the anvil after pressure release. (d)–(f) Anvils for ultrahigh-pressure hydrogen experiments, with the maximum pressures before failure being 210 GPa, 232 GPa, and 270 GPa, respectively.

hydrogen under ultrahigh pressures, we strove to maintain quasi-hydrostatic conditions by using highly compressible He as the pressure medium. Loubeyre *et al.*[41] proposed this novel idea and were able to preserve a relatively high quality of hydrogen crystal in helium up to 120 GPa. With a He pressure medium, we grew a single crystal of hydrogen near 6 GPa[41] and maintained it up to 158 GPa using diamond anvils with a 50 μm culet. To grow a visible crystallite of hydrogen, we had to maintain the size of the sample chamber at no less than 15 μm, so that a single crystallite ~5 μm in diameter could be made. With a small clean-up pinhole (e.g., 8 μm in diameter on the 13 IDD beamline at the APS), an XRD pattern without very strong diffraction from a metal gasket material can be obtained. Unfortunately, with such a sample configuration, the pressure was limited to below 158 GPa. Based on all our hydrogen-related experiments, we noticed that the maximum pressure was inversely proportional to the chamber size, as shown in Fig. 3. This result comes from samples with similar anvil culet sizes (40–50 μm) and gasket setups (Re or W gaskets). Similar observations were also reported by Howie *et al.*[22] in their Raman spectroscopy studies of hydrogen. Such a relationship makes sense, since a smaller chamber means that there is less contact between the highly diffusive sample (helium or hydrogen) and the diamond anvil surface, where a diffusive material may penetrate into microcracks (inset in Fig. 3), resulting in premature failure of the diamond anvil. As a result, small samples

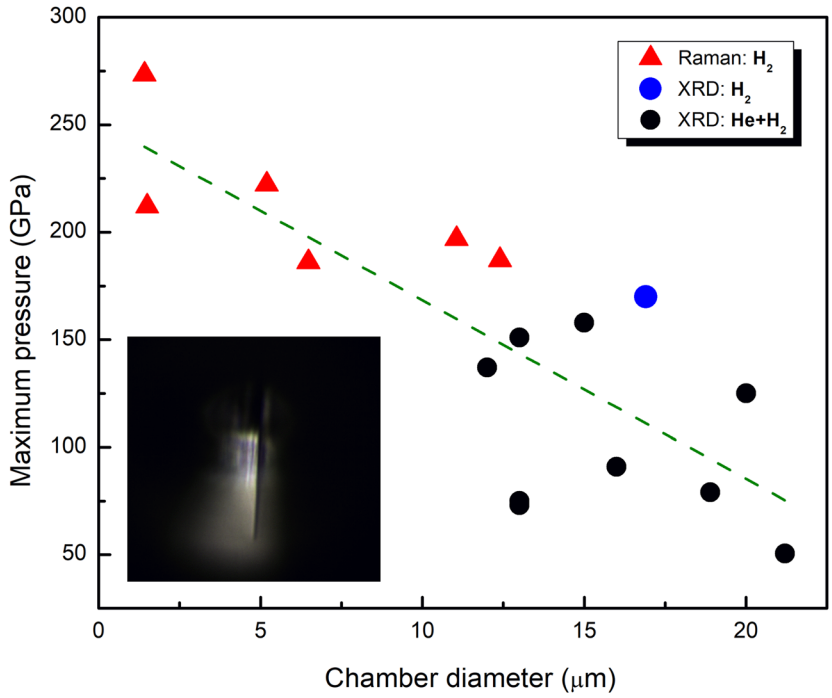

FIG. 3. Correlation of the maximum pressures achieved on hydrogen samples with the final sizes of the sample chambers. The inset shows a microscope image of a diffusion-induced crack inside a diamond anvil with a hydrogen sample at megabar pressure. This figure summarizes some of our early experiments with W gaskets and 40 or 50 μm culet diamond anvils. Later experiments with composite gaskets under similar experimental conditions are not included here.

are more suitable for achieving multimegabar pressure conditions, either for measuring XRD of solid hydrogen or for performing quasi-hydrostatic experiments with He as the pressure medium. Surface coating has been suggested as an option to prevent diffusion-induced diamond failures.[23,60] We avoided this method because of the risks of XRD signal from the coating materials (sample thickness vs coating thickness is approximately 20:1 at 2 Mbar pressure) and reaction between the coating materials and hydrogen. However, there is a problem in using small samples (~5 μm) for XRD experiments, namely, the strong diffraction background from gasket materials. Even though this can be solved by using an ultrasmall clean-up pinhole placed very near the sample, the presence of such an aperture physically restricts rotation of samples, making data collection with rotating samples difficult (such samples are required for SXRD data collection with a monochromatic X-ray beam).

D. X-ray transparent composite gasket

The problem of gasket XRD background from small samples is solved by using composite gaskets with light material inserts. Traditional metal gaskets, usually made of heavy metals such as Re and W, generate strong XRD signals when samples become small (<5 μm in diameter), since the X-ray beam profile has a tail that is usually larger than a 5 μm sample chamber, as demonstrated in Fig. 4. By using a composite gasket, light material inserts (cBN or MgO in our case), instead of heavy metal, surround a sample so that the X-ray tail does not graze heavy metal. As a technique previously used widely for electrical conductivity measurements at high pressures,[23] composite gaskets with light inserts are obviously quite suitable for XRD measurements at ultrahigh pressure, where the sample chamber size is small owing to the required small culet size. In our case, the use of composite gaskets enables us to perform SXRD collection by rotating the DAC around the Ω axis by ±20° (this angle is limited by the X-ray opening of the Boehler–Almax diamond anvils that we used) while achieving an extremely clean background. This technique can be readily extended to improve data quality in ultrahigh-pressure XRD studies of all materials, where strong gasket diffraction backgrounds can have very serious consequences.

The use of composite gaskets does lead to some difficulties in determining the sample position. Traditionally, the sample position is determined from the X-ray transmission contrast between the sample and the heavy metal gasket materials. However, light insert materials do not have enough transmission contrast compared with hydrogen, especially with hard X rays (we used energies ranging from 20 keV to 35 keV). Position determination for such samples can be performed more easily at beamlines that are equipped with online scopes coaxial with the X-ray beam to observe the DAC sample, such as the laser heating beamlines 16 IDB and 13 IDD at the APS and BL10XU at SPring8. However, when the sample is as small as ~5 μm and the pressure is high, visual identification becomes nontrivial. We used XRD contrast imaging to identify the sample position, as illustrated in Fig. 5. By tracking a selected Bragg peak of the gasket insert material [cBN in the case of Fig. 5(c)], the intensity map is able to resolve exactly the location of the hydrogen sample [Fig. 5(d)]. Subsequent SXRD data collection can be performed precisely at locations inside the sample chamber.

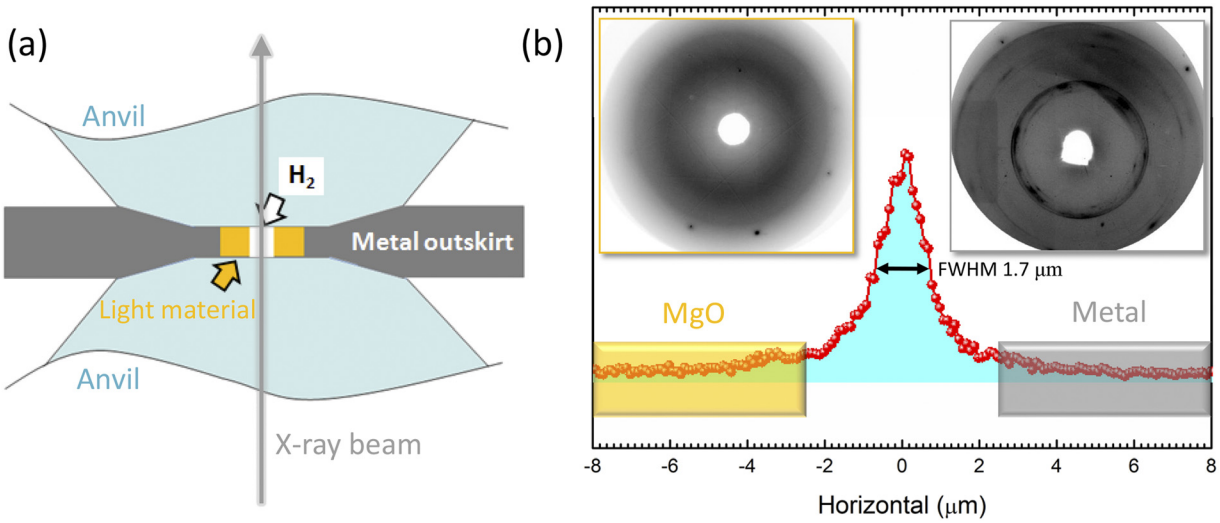

FIG. 4. (a) Schematic of the X-ray path of a sample in a DAC with a composite gasket. (b) Demonstration of the influences of the tail of a focused X-ray on XRD patterns from DAC samples. The inserts on the left and right show XRD patterns in the case of a composite gasket with an MgO insert and the case of a Re gasket, respectively.

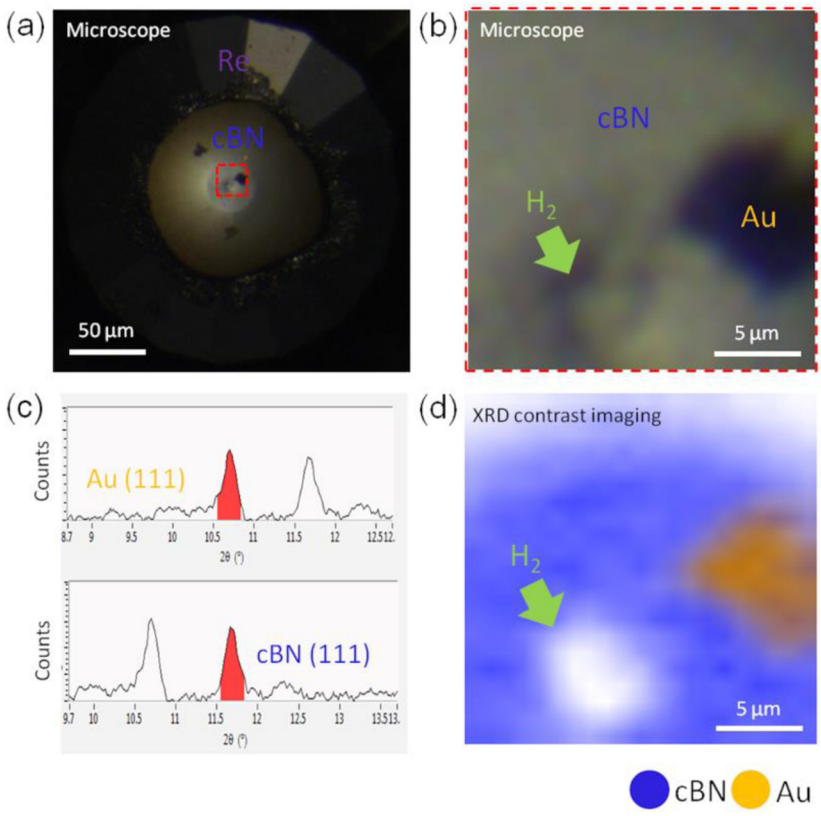

FIG. 5. XRD contrast imaging of a hydrogen sample with a composite gasket. (a) Microscope image of the sample illustrated by both transmitted and reflected light. (b) Enlarged image of the part included in the red dashed box in (a). (c) Bragg peaks tracked in XDI software.[53] Red shading marks the Bragg peaks from which the intensity is subtracted. (d) XRD contrast image of the same sample area corresponding to (b). Blue and orange represent cBN and Au, respectively. Darker color represents higher Bragg peak intensity. The white area corresponds to hydrogen.

E. XRD techniques for investigating solid hydrogen at ultrahigh pressures

We systematically experimented with three methods for XRD measurements on hydrogen: (1) a hydrogen single crystal grown in He medium (H_2–He sample) using a micrometer beam; (2) a pure-H_2 sample using a nano beam; (3) a pure-H_2 sample using a micrometer beam and an MCC. In fact, we also tried to perform a powder XRD study of hydrogen, with the DAC being static, above 200 GPa with a long exposure time (30 min) on 16 IDB, but this did not yield any identifiable hydrogen XRD signal. As a result, we skip the details of these powder XRD trials here. The first method has the advantage of preserving relatively large single crystals, but it is not suitable for measurements above 200 GPa, owing to some fatal drawbacks. The second and third methods worked for measurements above 200 GPa, even though hydrogen crystallites defragmented into submicrometer grains. We discuss the details of each method below.

The first method investigates deformed single crystals of hydrogen, 5–10 μm in diameter and 1–2 μm thick, embedded in He pressure media using a microfocused X-ray beam (typically 6×7 μm^2). H_2–He samples were typically loaded with an Au pressure marker using heavy metal gaskets (Re or W), as shown in Fig. 6(a). A single crystal was first grown at 5.7 GPa at RT, with fine control to place the crystal at the center of a sample chamber. Compared with the previous study where this method was invented,[41] the culet size of the diamond anvils was scaled down to achieve higher pressures. For instance, the size of the sample chamber at 14 GPa in the previous study was approximately 50 μm,[41] whereas the culet size in our study was 50 μm, with the chamber size being ~15 μm. An XRD study of hydrogen up to 158 GPa used a micrometer focused X-ray beam [7×6 μm^2, 3×2 μm^2, or 2×2 μm^2 at full width half maximum (FWHM)]. The data were collected by rotating the –DAC from –20° to 20° in steps of 0.5°. In fact, all three methods in this section require SXRD data collection. Figure 6(b) shows XRD images of six arc-shaped (100) hydrogen Bragg peaks measured with 1 s exposure at 158 GPa. By transforming these peaks (arc center) into reciprocal space [Fig. 6(c)], the (100) reciprocal lattice points are coplanar, with angles between adjacent points close to 60°. No obvious distortion can be inferred in the basal plane of the hcp lattice up to 158 GPa. The single crystal appears to be deformed, with the rocking curve being ~2° and arc-like Bragg peaks spanning azimuthal angles of ~3° [Figs. 6(d) and 6(e)]. This is in sharp contrast to the data quality obtained using a nano-focused X-ray beam, which will be demonstrated later. Although the H_2–He single-crystal method allows XRD measurements of hydrogen up to 158 GPa, it has two major problems. First, the size of the sample chamber is supposed to be maintained at least 10–15 μm for growing sizable single crystals of hydrogen in He. As suggested in Fig. 3, the relatively large sample chamber increases the probability of premature failures of anvils due to diffusion of H_2 or He. This explains our difficulties in achieving pressures beyond 158 GPa at RT. A pressure of only

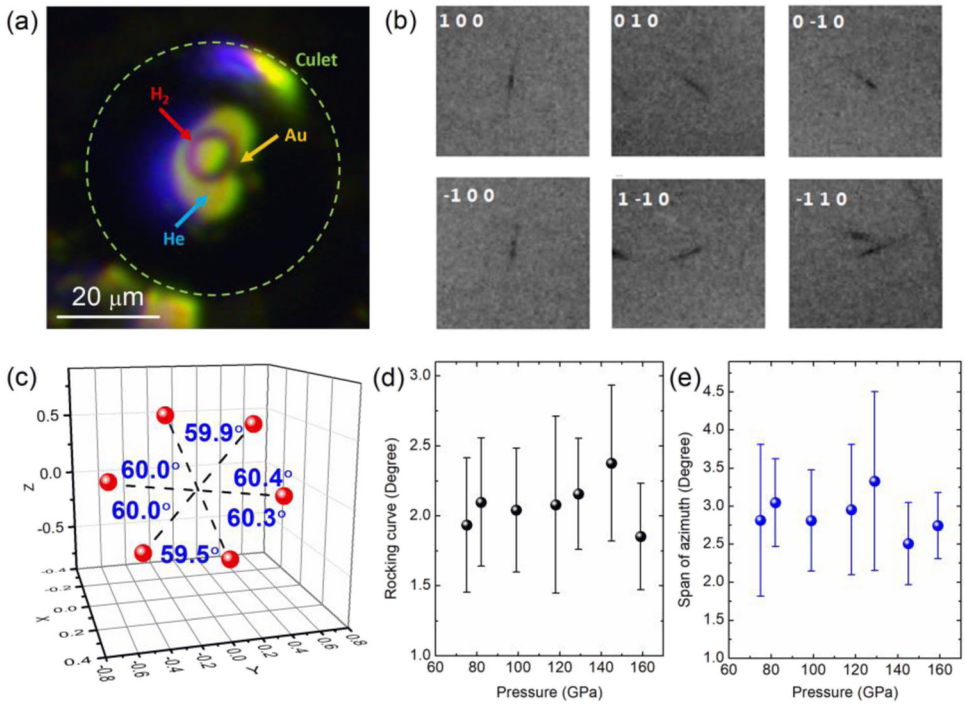

FIG. 6. (a) Microscope image of a typical H_2–He sample with 40 or 50 iμm culet. (b) Raw XRD images (exposure time 1 s) of measured hydrogen (100) reflections at 158 GPa. Numbers represent Miller indices for each reflection. (c) Measured (100) reflections at 158 GPa in reciprocal space. The angles marked are those between adjacent reciprocal lattice points. Dashed lines are visual guides. (d) Evolution of rocking curve of (100) reflections with pressure. (e) Span of the diffraction arc in azimuth angle. Error bars in both (d) and (e) stand for the standard deviation of the six (100) reflections.

158 GPa appears to fall far short of the full potential of diamond anvils with 50 μm culets to achieve high pressures. In addition, a strong preferred orientation of a hydrogen single crystal is usually present at megabar pressures, with the c axis of the hcp unit cell aligning with the compression axis (see Fig. S1 in the supplementary material), restricting the measurement of reflections other than the (100) reflections. This leads to great difficulties in obtaining the complete set of unit cell parameters. The other two methods were explored to circumvent these problems.

The second method probes submicrometer hydrogen crystallites using a nano-focused X-ray beam. Instead of growing single crystals of hydrogen in a He medium, small chambers (~5 μm in diameter) filled with pure hydrogen were loaded using composite gaskets. In contrast to the previous idea of growing a sizable single crystal of hydrogen for probing, in this method, a nano beam is used to pick up submicrometer single crystallites[61] in a defragmented sample. With such an X-ray probe, photons are focused onto particular crystallites of hydrogen, satisfying the Bragg condition and cutting off photons on nondiffracting crystallites, which only build up background (Compton scattering from diamonds in the beam path). We used two focus sizes (FWHM), namely, 300 nm at 24 keV (on the 34 IDE beamline at the APS) and 50 nm at 20 keV (on NanoMAX at MAX IV). Performing SXRD data collection using the rotational method (rotating the DAC in the range of ±20° in steps of 0.2° or from 0° to 20° in steps of 0.1°), resolves round and sharp hydrogen Bragg peaks, which can be clearly identified. Figure 7(a) shows a typical XRD raw image containing a Bragg peak from hydrogen. The data were obtained on NanoMAX. A presentation of 34 IDE data can be found in our previous work.[44] With a 50 nm X-ray beam, usually a couple of Bragg peaks can be resolved, whereas a 300 nm X-ray beam captures dozens of peaks. The grain size of crystallites, analyzed by two-dimensional XRD contrast imaging, is shown to be sub-micrometer, as illustrated in Figs. 7(e) and 7(f). Since the beam size is less than the grain size, the probed sample area exhibits low mosaic spread in XRD data. The smaller the X-ray beam, the sharper is the rocking curve. For instance, the rocking curve is approximately 0.2° in Ω with the 50 nm X-ray beam, whereas it is typically 0.4° when the 300 nm X-ray beam is used. The quality of the data obtained with the nano beam is obviously much higher than that of the data collected from the H_2–He samples using a micrometer-focused X-ray beam, from three aspects. First, the profile of the Bragg peaks becomes round and sharp [Fig. 7(b)], in contrast to an arc-like profile [Fig. 6(b)]. Second, the rocking curve is more than 10 times sharper [Figs. 7(g) and 7(h) vs Fig. 6(d)]. Third, the signal-to-background ratio (SBR) is significantly improved, owing to the fact that the illuminated portion of the hydrogen crystal has improved crystalline quality when the X-ray beam becomes small enough. We have successfully measured

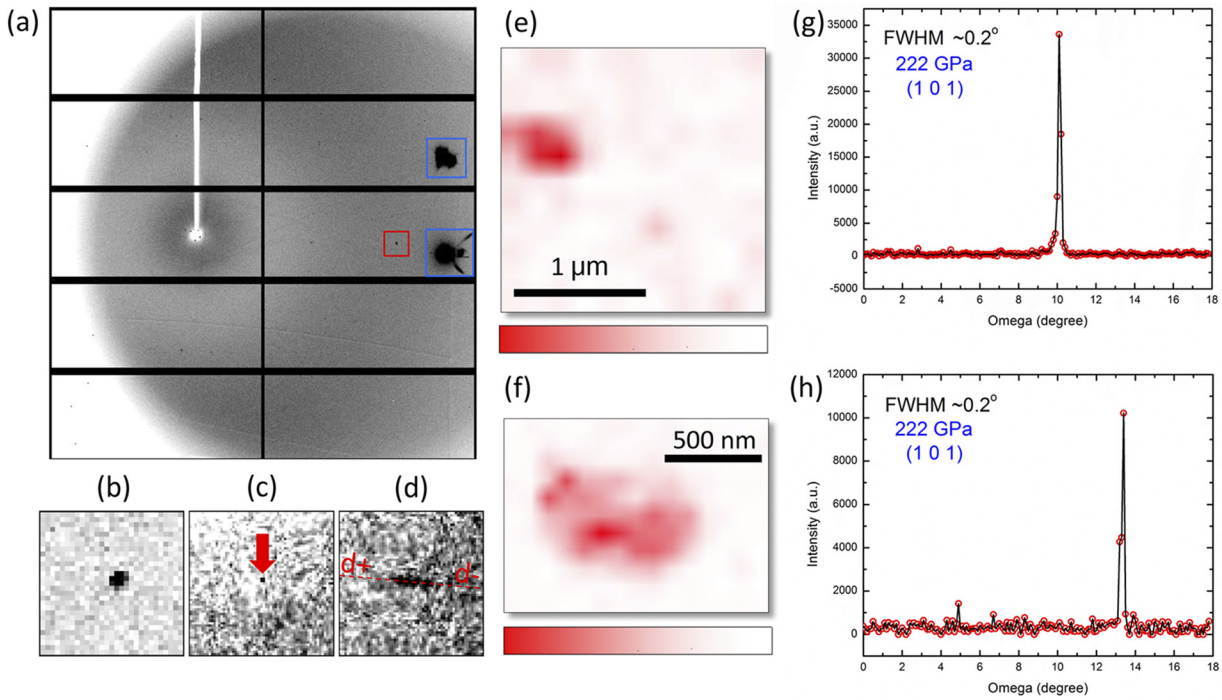

FIG. 7. XRD of hydrogen using a 50 nm focused X-ray beam. (a) Selected XRD raw image showing the Bragg peak of hydrogen (red box). The saturating Bragg peaks (blue boxes) are from diamond. (b), (c), and (d) Cropped XRD images of a hydrogen Bragg peak and two types of non-sample peaks, respectively. The image in (b) was obtained from a Pilatus 1M detector with 172 μm pixel size, and those in (c) and (d) were obtained from a MarCCD detector with 79 μm pixel size (300 nm X-ray beam). (e) and (f) XRD contrast imaging of hydrogen crystallites at 198 GPa. Darker color represents stronger Bragg peak intensity. The step size in both the horizontal and vertical directions is 100 nm. (g) and (h) Typical rocking curves of hydrogen Bragg peaks at 222 GPa.

XRD of hydrogen up to 254 GPa using a nano beam.[44] On further compression, the submicrometer crystallites, embedded in a soft hydrogen pressure medium, are not likely to break down quickly. Thus, using a finely focused nano beam to resolve XRD from solid hydrogen at higher pressures is promising, as long as the grain size remains above the size of the X-ray probe. At present, there are two major shortcomings of this technique. The first is the difficulty in locking on and measuring a particular single crystallite while rotating the sample through a large angular range. The second is the lack of detectable reflections beyond (101) at high scattering angles. Both of these shortcomings prevent single-crystal refinement of the crystal structure. Further technical developments, such as ultrahigh-precision rotation stages, precision translation stages that generate low heat (piezo-stages with enough load capacity), and better hutch temperature control, are required to break through the first technical barrier, while developments of diagnostic methods for further improving SBR (such as the use of an MCC, which will be discussed below, and detectors with higher quantum efficiency as well as lower background) are expected to tackle the second technical problem. Recently, Ackland and Loveday[62] provided simulated XRD patterns of hydrogen high-pressure phases, emphasizing fine differences between new models and the hcp model in the form of extra peaks weaker than 100, 002, and 101 peaks of hcp. Future technical developments are also necessary to allow better examination of these models.

We explain here our use of the term "single-crystal" XRD, about which concerns have been raised.[63] In fact, we used a nano X-ray beam impinging upon a submicrometer hydrogen "single crystal" that produced discrete, round Laue spots, instead of powders, which would have produced smooth rings. By definition, this is "single-crystal" XRD and is currently almost the only way (a micrometer beam with a MCC also works, as explained below) that *d* spacings, although not the orientation, can be obtained for hydrogen at 250 GPa.

We also emphasize that the identification of hydrogen Bragg peaks is critical in data processing of the XRD data using a nano beam. Some doubts regarding the identification of hydrogen peaks in our work[44] have been raised.[63] In the comments in Ref. 63, spots other than hydrogen peaks were highlighted on the XRD image and questioned. In fact, all of the marked spots had already been examined previously and deemed not to belong to hydrogen. Unlike ordinary

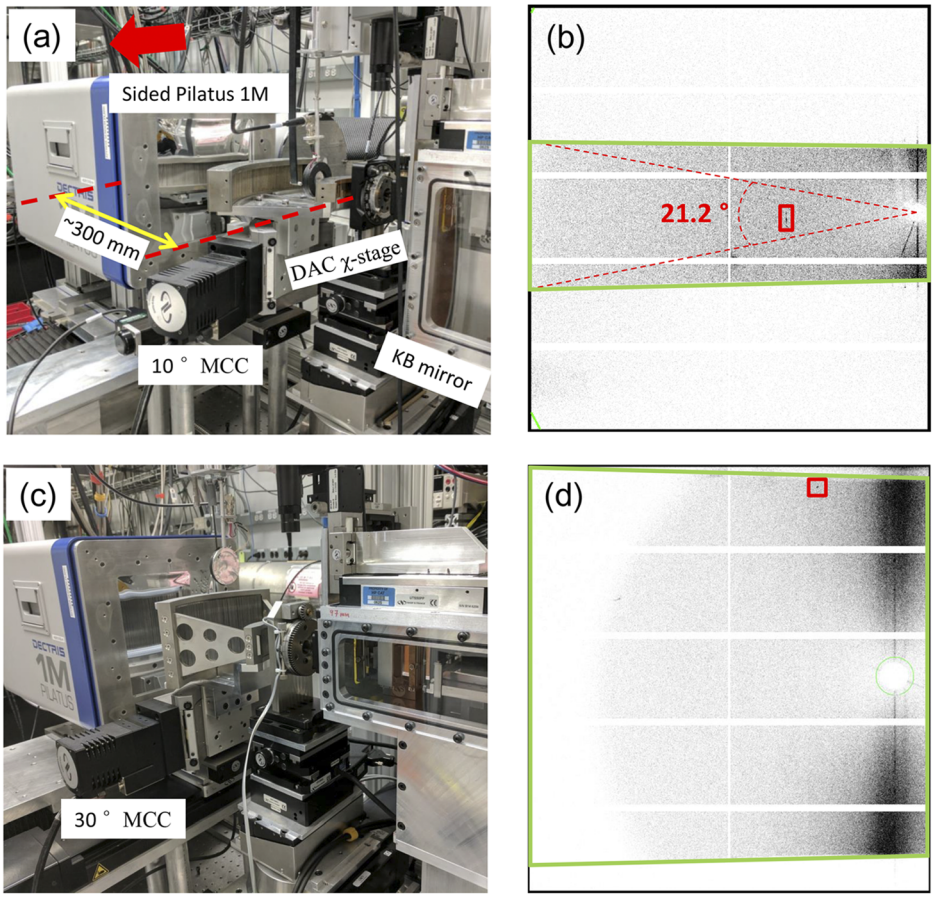

FIG. 8. (a) Experimental setup with the 10° MCC and (b) example of an XRD image obtained with it. (c) Experimental setup with the 30° MCC and (d) example of an XRD image obtained with it. Experimental devices were pictured at 16IDB of APS, ANL. The green and red boxes in (c) and (d) mark the exposed areas on the Pilatus 1M detector from the MCCs and hydrogen Bragg peaks, respectively.

high-pressure experiments, where the XRD spots from a single-crystal sample overwhelmingly stand out and the weak background spots are often ignored, the valuable signals from submicrometer hydrogen crystals are relatively weak and must be carefully searched for. Meanwhile, with low-SBR data, ordinarily insignificant background spots can become visible and must be thoroughly analyzed and discriminated. Therefore, the critical first step in our data processing of low-SBR images was to analyze each spot to verify whether it was a signal from hydrogen, which must satisfy four criteria, namely, reproducibility (the same peak appears in another crystallite), spot shape (usually round owing to the hydrostaticity of hydrogen, but sometimes in the form of a short arc owing to some strain within the X-ray covered area), reasonable peak width (integrated over 2θ), and reasonable rocking curve (rotational XRD data collection was performed). Taking the data at 232 GPa for example (with a 300 nm X-ray beam),[44] the peak width and rocking curve (both FWHM) of a typical hydrogen Bragg peak are $0.1^\circ \pm 0.01^\circ$ in 2θ and $0.3^\circ \pm 0.1^\circ$ in Ω (rotation axis), respectively. We have verified good statistical reproducibility and observed 40 spots of hydrogen that have similar peak widths and rocking curves, and can be indexed to 100 (8 peaks), 002 (5 peaks), and 101 (27 peaks) of the hcp unit cell. In addition, spots originating from electronic noise can be distinguished by their sharp peaks within a couple of pixels, as demonstrated in Fig. 7(c). Very broad spots with FWHM of 2θ greater than 0.2° [Fig. 7(d)] and very wide rocking curves (spanning tens of degrees in Ω) are related to the highly strained diamond anvil or to gasket materials and their multiple scattering. Spots generated by cosmic rays and other singular events are not reproducible. These criteria would in general also be valid for studying XRD of low Z materials using a nano beam.

The third method uses a micrometer X-ray beam ($6 \times 7\ \mu m^2$ or $1 \times 2\ \mu m^2$) coupled with an MCC on pure-H_2 samples with composite gaskets. The MCC is able to suppress the Compton scattering by the diamond anvil, which is the dominant source of background in our XRD measurements. MCCs have been applied to high-pressure studies of liquid and amorphous materials[64–67] using either large volume presses or DACs. Our experiments suggest that Compton scattering from diamond anvils is significantly reduced by as much as 83% at 1.5 Å (see Fig. S2 in supplementary material). The reduction in background is q-dependent, with the reduction increasing at larger q. Owing to the improved SBR, we were able to measure a pure hydrogen sample in the same sample configurations as the nano beam measurements. However, MCCs for high-pressure studies were originally designed for measuring liquids in large volume presses. The vertical opening angle of a MCC is limited (10° in our case). This is not a problem for liquid X-ray scattering or powder XRD, but introduces increased operational complexity in SXRD measurements. Explicitly, when an MCC with a 10° vertical opening [Fig. 8(a)] was used, the DAC sample stage has to offer an additional rotational degree of freedom in the χ axis (the direction coinciding with the compression axis of the DAC). A single-crystal grain has to be prealigned in the χ axis at low pressure, so that the targeted Bragg peaks penetrate through the MCC opening to be exposed on the Pilatus 1M detector (only one-third of the detector is available), as shown in Fig. 8(b). Compression can then be applied, provided that the identified peaks remain trackable. A blind search of Bragg peaks at ultrahigh pressure using SXRD data collection with such an MCC is very difficult, since the SXRD data collection has to be repeated either at different χ angles by rotating the sample or at different detector positions by moving the area detector up and down. Considering that data collection with an MCC is itself time-consuming, such operations are almost impractical. At HPCAT, we developed a special MCC with three times larger vertical opening angle (30°) to solve this problem, as shown in Fig. 8(c). Such an MCC allows photons to pass through and cover almost the entire Pilatus 1M detector. The search for hydrogen Bragg peaks can thus be performed directly at ultrahigh pressures. The red box in Fig. 8(d) outlines an example of a captured hydrogen Bragg peak at 240 GPa, which would have been out of sight if the 10° MCC had been used. With the improved MCC, we were also able to measure XRD of hydrogen up to 250 GPa.[44]

The competition between the XRD signals of hydrogen and the background determines the success of measurements. Here, we

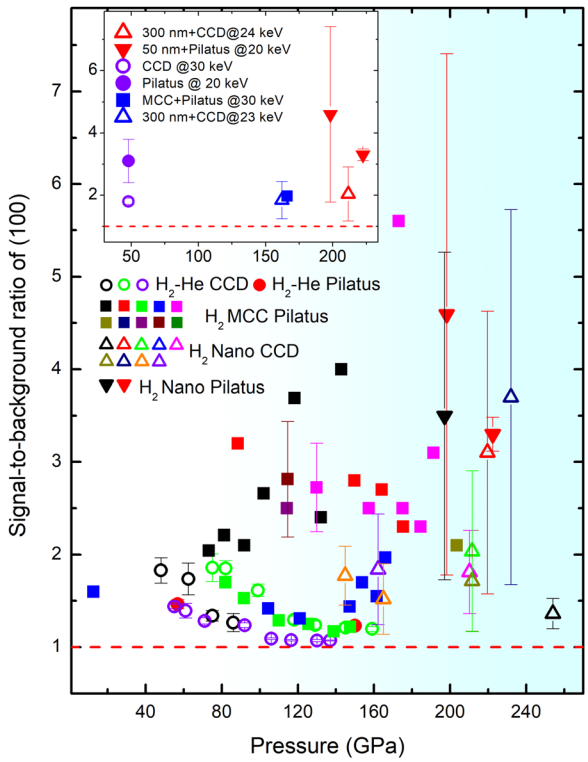

FIG. 9. Comparison of the SBR [hydrogen (100)] for different setups. Open and solid symbols represent data collected using MarCCD 165 and Pilatus 1M detectors, respectively. Circles represent H_2–He samples measured using a $6 \times 7\ \mu m^2$ (30 keV) or $3 \times 2\ \mu m^2$ (37 keV) focused X-ray beam. Squares are data measured on pure-H_2 samples using an MCC, probed by $6 \times 7\ \mu m^2$ focused X-ray beam at 30 keV (10° MCC). Upward-pointing triangles are data measured on pure-H_2 samples using a 300 nm focused X-ray beam at 23 keV or 24 keV. Downward-pointing triangles are data measured on pure-H_2 samples using a 50 nm focused X-ray beam at 20 keV. The inset shows a comparison of SBRs measured with different setups on same samples. Symbols with the same color were measured from one particular sample. The detailed conditions are described in the key. Data obtained with the MCC usually lack an error bar since only one (100) Bragg peak was resolved. Data obtained with the nano beam may have large error bars since several Bragg peaks from crystallites in different qualities were measured.

compare the SBR by using different techniques to help understand how to better perform measurements at higher pressures. Figure 9 shows the evolution of the SBR with pressure according to different techniques. The SBR describes the averaged intensity of a hydrogen Bragg peak against the averaged background intensity around the targeted peak. When SBR drops to 1, no Bragg peak can be distinguished from the background. Figure S3 (supplementary material) explains how the SBR was calculated. The H_2–He method shows the lowest SBR (represented by circles in Fig. 9), which dropped to ~1.2 at 158 GPa [the corresponding raw XRD images can be found in Fig. 6(b)]. Use of the MCC significantly improves the SBR. It is noticeable that the MCC data (squares) appear very scattered, which is mainly due to two reasons associated with the significantly long exposure time when an MCC is used (an MCC allows only one-tenth of the X-ray photons to pass through it). First, for the data measured using a 10° MCC (the majority of the MCC data), only one (100) peak and one (101) peak were measured for each sample, and the SBR depended heavily on the quality of the measured crystal and varied among different samples. Second, we did not optimize the SBR of a Bragg peak by rocking in Ω, in order to minimize X-ray exposure. Minimization of exposure time is not only for saving precious beamtime: more importantly, we noticed that high-brilliance X rays appear to be harmful to highly stressed diamond anvils. The use of a nano beam also apparently increases the SBR. Some strong Bragg peak achieved SBR values as high as 10, which is 8 times stronger than the SBR measured with the H_2–He method (at even lower pressures). The error bars of nano beam samples are generally large, since many of the Bragg peaks that were measured originated from different hydrogen crystallites with diverse crystalline qualities. We picked three samples, measured with different techniques, which provide data as control groups, and plotted the results in the inset of Fig. 9. It can be seen from the purple symbols that use of the Pilatus 1M detector at 20 keV apparently improves the SBR compared with that obtained with the MarCCD detector at 30 keV. The effect of using a 300 nm beam is comparable to that using an MCC with a 1×2 μm^2 beam (blue symbols), while the use of a smaller nano beam (50 nm) coupled with the Pilatus 1M seems to improve the SBR compared with that using a 300 nm beam with the MarCCD (red symbols). However, because we knew that both the 300 nm and 50 nm beam sizes are smaller than the grain size of the crystallites, the increased SBR with 50 nm beam plus Pilatus may be a mere consequence of using different detectors (as already suggested by the purple circles). Guided by the above results, future experiments could be optimized by combining a nano-focus beam, an MCC, and a low-background detector (CCDs have high electronic noise when the exposure time becomes long). High quantum efficiency at high energy and large area are desirable for the detectors to ensure high q-coverage, since the use of an MCC significantly increases sample-to-detector distance, as shown in Fig. 8(a). At much higher pressures, a 50 nm or even smaller beam would be very useful when crystallites undergo further significant breakdown.

F. Pressure scales at ultrahigh pressures

Accurate measurement of very high pressures remains a difficult task, because there is no generally accepted single best pressure calibration over this pressure range. We used multiple, redundant calibrations (six independent pressure calibrations) under their optimal conditions, namely, the ruby fluorescence scale at low pressures, the Au scale[47] up to 160 GPa, the MgO scale[68] when an MgO gasket was used, the hydrogen d_{100} scale over the entire pressure range, the diamond Raman edge,[69] and the hydrogen Raman vibron[27] as a cross check before and after synchrotron XRD when the sample survived. We were able to establish pressure consistency among these calibrations within their individual accuracies. The d_{100} scale, which was calibrated against the EOS of Au up to 158 GPa, is our preferred pressure scale because it can unify all data under the same scale. To ensure that extrapolation of this scale above the pressures of the phase

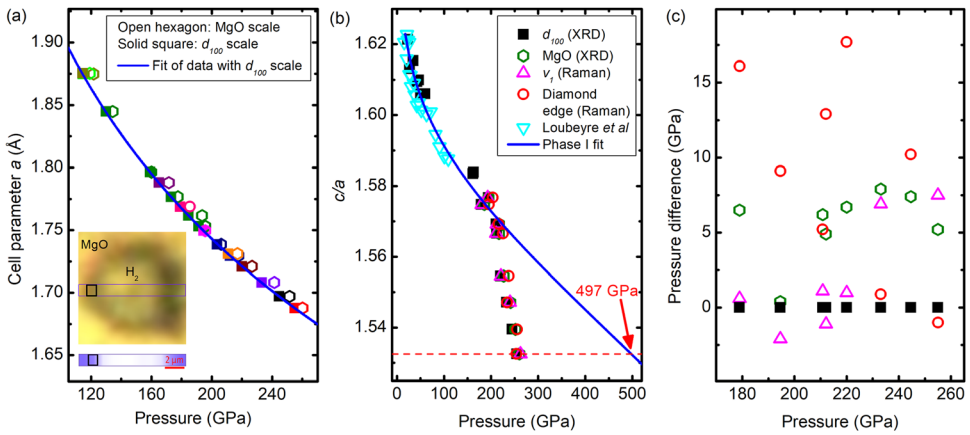

FIG. 10. (a) Comparison between the d_{100} pressure scale and the MgO pressure scale. Solid squares and open hexagons represent data on the d_{100} and MgO pressure scales, respectively, with different colors representing different runs. The blue curve is a fit of data on the d_{100} scale. The inset shows a microscope image (top) and an XRD contrast image (bottom) of a sample. The pressure on the MgO gasket is measured at the position inside the black box, where MgO is in direct contact with hydrogen. (b) Comparison of different pressure scales in terms of c/a. Solid squares, open hexagons, open upward-pointing triangles, open circles, and open downward-pointing triangles represent data on the d_{100} scale, MgO scale,[68] Raman shift of v_1 scale,[27] diamond edge scale,[69] and the reference from Loubeyre *et al.*,[41] respectively. The blue curve is a fit of phase I data on the d_{100} scale. The red dashed line serves as a visual guide. (c) Differences between the d_{100} scale and the other scales. The key to the symbols is the same as that for (b). Part of (a) and (c) is adapted from Fig. 6 of our.[70]

transitions is still valid, we first compared the d_{100} scale against the MgO scale, as shown in Fig. 10(a). The pressure from the MgO scale is measured at the position of the MgO gasket in direct contact with hydrogen [inset of Fig. 10(a)]. The comparison demonstrates that the d_{100} shifts smoothly across the I–III–IV phase transitions without obvious discontinuity, proving that the extrapolation of the P–d_{100} relationship up to 254 GPa for determining pressure is valid. This answers the concern[63] raised about the use of the d_{100} pressure scale for phase III and IV conditions. The use of the extrapolated Au-calibrated d_{100} scale is better than the use of the MgO scale, because the pressure from the MgO in the gasket [the pressures in Fig. 2(e) in our recent work[44]] should be systematically slightly higher (5–10 GPa) than the pressure of the adjacent hydrogen sample. We further compared our calibrated P–d_{100} relationship with the MgO scale,[68] diamond Raman edge,[69] and hydrogen Raman vibron scale.[27] As demonstrated by the P–c/a relationship in Fig. 10(b), these scales are generally consistent, resolving a kink suggesting the onset of phase IV. The kink is thus proved to be real, rather than being a consequence of "objective characterization of pressure and the graphical presentation of the data."[63] If the kink in the P–c/a curve is ignored, our highest-pressure experimental data would correspond to 497 GPa [shown graphically in Fig. 10(b)], which is simply impossible and contradicts all other data. Comparison of the pressure values with the d_{100} scale as reference shows that the hydrogen Raman vibron scale[27] is closest to the d_{100} scale (both scales reflect pressures in hydrogen). Above 200 GPa, the MgO scale systematically overestimates the pressure by 3%–4%, while the diamond edge scale can differ with the d_{100} scale by up to 9%. The diamond edge scale scatters the most since the measured values depend on the specific sample configurations, namely, anvil geometry, gasket material, gasket geometries, etc. We extrapolated the P–d_{100} scale up to 400 GPa, as shown in Table S1 (supplementary material). We expect the applicability of this pressure scale in this pressure range not to be significantly affected only by two previously reported phase transitions at higher pressures, namely, phases IV′ (270 GPa)[24] and V (325 GPa),[25] which are believed to experience little structural modification compared with phase IV (220 GPa). To be cautious, however, further cross checking of the P–d_{100} scale against other scales, as we have done, is expected at higher pressures.

IV. SUMMARY

We systematically studied the methods for performing synchrotron XRD measurements on solid hydrogen under extreme compression. These methods allowed us to successfully determine the crystal structure of solid hydrogen up to 254 GPa at RT.[44] In this paper, a bottom-up analysis ranging from the selection of diamond anvils to XRD diagnostic techniques has been presented, providing references for future synchrotron XRD experiments on solid hydrogen, as well as other materials (especially those with low Z), at ultrahigh pressures. X-ray transparent composite gaskets would be useful for obtaining clean XRD data at multimegabar pressures when anvils with small culets (<50 μm) are used. This would greatly facilitate the determination of crystal structures of materials at pressures above 200 GPa, where the use of traditional metal gaskets gives XRD patterns that always contain a mixture of sample Bragg peaks and gasket peaks (quite often very strong). The use of a nano beam or an MCC improves the SBR of the XRD signal, allowing weak signals from submicrometer hydrogen crystallites to be made visible. These methods will be readily extendible to studies of other materials, since hydrogen is the weakest X-ray scatterer. With new techniques continuing to emerge, such as toroidal anvils[14,15] and the new generation of synchrotron X-ray sources,[71] ultrahigh-pressure crystallographic studies of materials can be taken to the next level.

SUPPLEMENTARY MATERIAL

See supplementary material for discussions on possible electronic topological transition in hydrogen.

ACKNOWLEDGMENTS

This research was supported by the National Natural Science Foundation of China under Award No. U1930401 and by the Department of Energy (DOE), Office of Basic Energy Science, Division of Materials Sciences and Engineering under Award No. DE-FG02-99ER45775. Portions of this work were performed on the following beamlines: 34 IDE, 16 IDB (HPCAT), 13 IDD (GSECARS), and 1 BM of the APS at ANL in the USA; BL15U1 of the SSRF in China; NanoMAX of MAX IV in Sweden; and BL10XU of SPring8 in Japan (under Proposal No. 2019A1191). HPCAT operations are supported by the DOE and the National Nuclear Security Administration under Award No. DE-NA0001974. V.B.P. is grateful for the NSF MRI No. EAR/IF1531583 award. GSECARS is supported by the National Science Foundation—Earth Sciences (Grant No. EAR - 1634415) and the Department of Energy—Geosciences (Grant No. DE-FG02-94ER14466). This research used resources of the Advanced Photon Source, a U.S. DOE Office of Science User Facility operated for the DOE Office of Science by Argonne National Laboratory under Contract No. DE-AC02-06CH11357. The MAX IV Laboratory receives funding through the Swedish Research Council under Grant No. 2013-02235. The part of this research conducted at the SPring-8 facility is under Proposal Nos. 2019A1191 and 2019B1242. A.M., R.A., and W.L. would like to acknowledge support from the Carl Tryggers Stiftelse for Vetenskaplig Forskning (CTS), Olle Engkvists Stiftelse, and the Swedish Research Council (VR). SNIC and HPC2N are also acknowledged for providing computing time. A.S. acknowledges financial support from the J. C. Kempe and Seth M. Kempes Minne Foundation through Grant No. JCK-1505.

REFERENCES

[1]R. Jeanloz, "Physical chemistry at ultrahigh pressures and temperatures," Annu. Rev. Phys. Chem. **40**, 237–259 (1989).

[2]Y. Ma, M. Eremets, A. R. Oganov, Y. Xie, I. Trojan, S. Medvedev, A. O. Lyakhov, M. Valle, and V. Prakapenka, "Transparent dense sodium," Nature **458**, 182–185 (2009).

[3]C.-S. Yoo, "Chemistry under extreme conditions: Pressure evolution of chemical bonding and structure in dense solids," Matter Radiat. Extremes **5**, 018202 (2020).

[4]D. Laniel, G. Geneste, G. Weck, M. Mezouar, and P. Loubeyre, "Hexagonal layered polymeric nitrogen phase synthesized near 250 GPa," Phys. Rev. Lett. **122**, 066001 (2019).

[5]D. Tomasino, M. Kim, J. Smith, and C.-S. Yoo, "Pressure-induced symmetry-lowering transition in dense nitrogen to layered polymeric nitrogen (LP-N) with Colossal Raman intensity," Phys. Rev. Lett. **113**, 205502 (2014).

[6]M. I. Eremets, A. G. Gavriliuk, I. A. Trojan, D. A. Dzivenko, and R. Boehler, "Single-bonded cubic form of nitrogen," Nat. Mater. **3**, 558–563 (2004).

[7]M. Somayazulu, M. Ahart, A. K. Mishra, Z. M. Geballe, M. Baldini, Y. Meng, V. V. Struzhkin, and R. J. Hemley, "Evidence for superconductivity above 260 K in lanthanum superhydride at megabar pressures," Phys. Rev. Lett. **122**, 027001 (2019).
[8]A. P. Drozdov, P. P. Kong, V. S. Minkov, S. P. Besedin, M. A. Kuzovnikov, S. Mozaffari, L. Balicas, F. F. Balakirev, D. E. Graf, V. B. Prakapenka, E. Greenberg, D. A. Knyazev, M. Tkacz, and M. I. Eremets, "Superconductivity at 250 K in lanthanum hydride under high pressures," Nature **569**, 528–531 (2019).
[9]C. J. Pickard and R. J. Needs, "*Ab initio* random structure searching," J. Phys.: Condens. Matter **23**, 053201 (2011).
[10]Y. Wang, J. Lv, L. Zhu, and Y. Ma, "Crystal structure prediction via particle-swarm optimization," Phys. Rev. B **82**, 094116 (2010).
[11]A. R. Oganov and C. W. Glass, "Crystal structure prediction using *ab initio* evolutionary techniques: Principles and applications," J. Chem. Phys. **124**, 244704 (2006).
[12]A. P. Drozdov, M. I. Eremets, I. A. Troyan, V. Ksenofontov, and S. I. Shylin, "Conventional superconductivity at 203 kelvin at high pressures in the sulfur hydride system," Nature **525**, 73–76 (2015).
[13]B. Li, C. Ji, W. Yang, J. Wang, K. Yang, R. Xu, W. Liu, Z. Cai, J. Chen, and H.-k. Mao, "Diamond anvil cell behavior up to 4 Mbar," Proc. Natl. Acad. Sci. U. S. A. **115**, 1713–1717 (2018).
[14]Z. Jenei, E. F. O'Bannon, S. T. Weir, H. Cynn, M. J. Lipp, and W. J. Evans, "Single crystal toroidal diamond anvils for high pressure experiments beyond 5 megabar," Nat. Commun. **9**, 3563 (2018).
[15]A. Dewaele, P. Loubeyre, F. Occelli, O. Marie, and M. Mezouar, "Toroidal diamond anvil cell for detailed measurements under extreme static pressures," Nat. Commun. **9**, 2913 (2018).
[16]L. Dubrovinsky, N. Dubrovinskaia, V. B. Prakapenka, and A. M. Abakumov, "Implementation of micro-ball nanodiamond anvils for high-pressure studies above 6 Mbar," Nat. Commun. **3**, 1163 (2012).
[17]A. Dewaele and P. Loubeyre, "Pressurizing conditions in helium-pressure-transmitting medium," High Pressure Res. **27**, 419–429 (2007).
[18]H.-k. Mao and R. J. Hemley, "Ultrahigh-pressure transitions in solid hydrogen," Rev. Mod. Phys. **66**, 671–692 (1994).
[19]I. F. Silvera and R. J. Wijngaarden, "New low-temperature phase of molecular deuterium at ultrahigh pressure," Phys. Rev. Lett. **47**, 39 (1981).
[20]X. D. Liu, R. T. Howie, H. C. Zhang, X. J. Chen, and E. Gregoryanz, "High-pressure behavior of hydrogen and deuterium at low temperatures," Phys. Rev. Lett. **119**, 065301 (2017).
[21]R. J. Hemley and H. K. Mao, "Phase transition in solid molecular hydrogen at ultrahigh pressures," Phys. Rev. Lett. **61**, 857 (1988).
[22]R. T. Howie, C. L. Guillaume, T. Scheler, A. F. Goncharov, and E. Gregoryanz, "Mixed molecular and atomic phase of dense hydrogen," Phys. Rev. Lett. **108**, 125501 (2012).
[23]M. I. Eremets and I. A. Troyan, "Conductive dense hydrogen," Nat. Mater. **10**, 927–931 (2011).
[24]R. T. Howie, T. Scheler, C. L. Guillaume, and E. Gregoryanz, "Proton tunneling in phase IV of hydrogen and deuterium," Phys. Rev. B **86**, 214104 (2012).
[25]P. Dalladay-Simpson, R. T. Howie, and E. Gregoryanz, "Evidence for a new phase of dense hydrogen above 325 gigapascals," Nature **529**, 63–67 (2016).
[26]P. Loubeyre, F. Occelli, and P. Dumas, "Hydrogen phase IV revisited via synchrotron infrared measurements in H_2 and D_2 up to 290 GPa at 296 K," Phys. Rev. B **87**, 134101 (2013).
[27]R. T. Howie, E. Gregoryanz, and A. F. Goncharov, "Hydrogen (deuterium) vibron frequency as a pressure comparison gauge at multi-Mbar pressures," J. Appl. Phys. **114**, 073505 (2013).
[28]A. F. Goncharov, I. Chuvashova, C. Ji, and H.-k. Mao, "Intermolecular coupling and fluxional behavior of hydrogen in phase IV," Proc. Natl. Acad. Sci. U. S. A. **116**, 25512–25515 (2019).
[29]P. Loubeyre, F. Occelli, and R. LeToullec, "Optical studies of solid hydrogen to 320 GPa and evidence for black hydrogen," Nature **416**, 613–617 (2002).
[30]C.-s. Zha, Z. Liu, M. Ahart, R. Boehler, and R. J. Hemley, "High-pressure measurements of hydrogen phase IV using synchrotron infrared spectroscopy," Phys. Rev. Lett. **110**, 217402 (2013).
[31]M. I. Eremets, I. A. Troyan, P. Lerch, and A. Drozdov, "Infrared study of hydrogen up to 310 GPa at room temperature," High Pressure Res. **33**, 377–380 (2013).
[32]C. S. Zha, Z. Liu, and R. J. Hemley, "Synchrotron infrared measurements of dense hydrogen to 360 GPa," Phys. Rev. Lett. **108**, 146402 (2012).
[33]P. Loubeyre, F. Occelli, and P. Dumas, "Synchrotron infrared spectroscopic evidence of the probable transition to metal hydrogen," Nature **577**, 631–635 (2020).
[34]C. J. Pickard and R. J. Needs, "Structure of phase III of solid hydrogen," Nat. Phys. **3**, 473–476 (2007).
[35]H. Liu, L. Zhu, W. Cui, and Y. Ma, "Room-temperature structures of solid hydrogen at high pressures," J. Chem. Phys. **137**, 074501 (2012).
[36]C. J. Pickard, M. Martinez-Canales, and R. J. Needs, "Density functional theory study of phase IV of solid hydrogen," Phys. Rev. B **85**, 214114 (2012).
[37]H. Liu and Y. Ma, "Proton or deuteron transfer in phase IV of solid hydrogen and deuterium," Phys. Rev. Lett. **110**, 025903 (2013).
[38]B. Monserrat, N. D. Drummond, P. Dalladay-Simpson, R. T. Howie, P. Lopez Rios, E. Gregoryanz, C. J. Pickard, and R. J. Needs, "Structure and metallicity of phase V of hydrogen," Phys. Rev. Lett. **120**, 255701 (2018).
[39]R. M. Hazen, H. K. Mao, L. W. Finger, and R. J. Hemley, "Single-crystal x-ray diffraction of n-H_2 at high pressure," Phys. Rev. B **36**, 3944–3947 (1987).
[40]H. K. Mao, A. P. Jephcoat, R. J. Hemley, L. W. Finger, C. S. Zha, R. M. Hazen, and D. E. Cox, "Synchrotron x-ray diffraction measurements of single-crystal hydrogen to 26.5 gigapascals," Science **239**, 1131–1134 (1988).
[41]P. Loubeyre, R. LeToullec, D. Hausermann, M. Hanfland, R. J. Hemley, H. K. Mao, and L. W. Finger, "X-ray diffraction and equation of state of hydrogen at megabar pressures," Nature **383**, 702–704 (1996).
[42]Y. Akahama, M. Nishimura, H. Kawamura, N. Hirao, Y. Ohishi, and K. Takemura, "Evidence from x-ray diffraction of orientational ordering in phase III of solid hydrogen at pressures up to 183 GPa," Phys. Rev. B **82**, 060101 (2010).
[43]Y. Akahama, Y. Mizuki, S. Nakano, N. Hirao, and Y. Ohishi, "Raman scattering and X-ray diffraction studies on phase III of solid hydrogen," J. Phys.: Conf. Ser. **950**, 042060 (2017).
[44]C. Ji, B. Li, W. Liu, J. S. Smith, A. Majumdar, W. Luo, R. Ahuja, J. Shu, J. Wang, S. Sinogeikin, Y. Meng, V. B. Prakapenka, E. Greenberg, R. Xu, X. Huang, W. Yang, G. Shen, W. L. Mao, and H.-K. Mao, "Ultrahigh-pressure isostructural electronic transitions in hydrogen," Nature **573**, 558–562 (2019).
[45]R. Boehler and K. De Hantsetters, "New anvil designs in diamond-cells," High Pressure Res. **24**, 391–396 (2004).
[46]R. Hrubiak, S. Sinogeikin, E. Rod, and G. Shen, "The laser micro-machining system for diamond anvil cell experiments and general precision machining applications at the High Pressure Collaborative Access Team," Rev. Sci. Instrum. **86**, 072202 (2015).
[47]O. L. Anderson, D. G. Isaak, and S. Yamamoto, "Anharmonicity and the equation of state for gold," J. Appl. Phys. **65**, 1534–1543 (1989).
[48]H. K. Mao, J. Xu, and P. M. Bell, "Calibration of the ruby pressure gauge to 800 kbar under quasi-hydrostatic conditions," J. Geophys. Res. **91**, 4673–4676 (1986).
[49]N. Hirao, S. I. Kawaguchi, K. Hirose, K. Shimizu, E. Ohtani, and Y. Ohishi, "New developments in high-pressure X-ray diffraction beamline for diamond anvil cell at SPring-8," Matter Radiat. Extremes **5**, 018403 (2020).
[50]C. Prescher and V. B. Prakapenka, "DIOPTAS: A program for reduction of two-dimensional X-ray diffraction data and data exploration," High Pressure Res. **35**, 223–230 (2015).
[51]M. Wojdyr, "Fityk: A general-purpose peak fitting program," J. Appl. Crystallogr. **43**, 1126–1128 (2010).
[52]J. Gonzalez-Platas, M. Alvaro, F. Nestola, and R. Angel, "EosFit7-GUI: A new graphical user interface for equation of state calculations, analyses and teaching," J. Appl. Crystallogr. **49**, 1377–1382 (2016).
[53]R. Hrubiak, J. S. Smith, and G. Shen, "Multimode scanning X-ray diffraction microscopy for diamond anvil cell experiments," Rev. Sci. Instrum. **90**, 025109 (2019).
[54]H. K. Mao, P. M. Bell, K. J. Dunn, R. M. Chrenko, and R. C. DeVries, "Absolute pressure measurements and analysis of diamonds subjected to maximum static pressures of 1.3-1.7 Mbar," Rev. Sci. Instrum. **50**, 1002–1009 (1979).

[55]X. R. Huang, M. Dudley, W. M. Vetter, W. Huang, W. Si, and C. H. Carter, Jr., "Superscrew dislocation contrast on synchrotron white-beam topographs: An accurate description of the direct dislocation image," J. Appl. Cryst. **32**, 516–524 (1999).
[56]X. Huang and A. T. Macrander, AIP Conf. Proc. **1234**, 191 (2010).
[57]Y. V. Shvyd'ko, S. Stoupin, A. Cunsolo, A. H. Said, and X. Huang, "High-reflectivity high-resolution X-ray crystal optics with diamonds," Nat. Phys. **6**, 196–199 (2010).
[58]A. Dewaele, P. Loubeyre, R. André, and J. Härtwig, "An x-ray topographic study of diamond anvils: Correlation between defects and helium diffusion," J. Appl. Phys. **99**, 104906 (2006).
[59]H. K. Mao and R. J. Hemley, "Optical transitions in diamond at ultrahigh pressures," Nature **351**, 721–724 (1991).
[60]R. P. Dias and I. F. Silvera, "Observation of the Wigner-Huntington transition to metallic hydrogen," Science **355**, 715–718 (2017).
[61]L. Wang, Y. Ding, W. Yang, W. Liu, Z. Cai, J. Kung, J. Shu, R. J. Hemley, W. L. Mao, and H.-k. Mao, "Nanoprobe measurements of materials at megabar pressures," Proc. Natl. Acad. Sci. U. S. A. **107**, 6140–6145 (2010).
[62]G. J. Ackland and J. S. Loveday, "Structures of solid hydrogen at 300 K," Phys. Rev. B **101**, 094104 (2020).
[63]L. Dubrovinsky, N. Dubrovinskaia, and M. I. Katsnelson, "No evidence of isostructural electronic transitions in compressed hydrogen," arXiv:1910.10772 (2019).
[64]K. Yaoita, Y. Katayama, K. Tsuji, T. Kikegawa, and O. Shimomura, "Angle-dispersive diffraction measurement system for high-pressure experiments using a multichannel collimator," Rev. Sci. Instrum. **68**, 2106–2110 (1997).
[65]M. Mezouar, P. Faure, W. Crichton, N. Rambert, B. Sitaud, S. Bauchau, and G. Blattmann, "Multichannel collimator for structural investigation of liquids and amorphous materials at high pressures and temperatures," Rev. Sci. Instrum. **73**, 3570–3574 (2002).
[66]G. Weck, G. Garbarino, S. Ninet, D. Spaulding, F. Datchi, P. Loubeyre, and M. Mezouar, "Use of a multichannel collimator for structural investigation of low-Z dense liquids in a diamond anvil cell: Validation on fluid H_2 up to 5 GPa," Rev. Sci. Instrum. **84**, 063901 (2013).
[67]C. Prescher, V. B. Prakapenka, J. Stefanski, S. Jahn, L. B. Skinner, and Y. Wang, "Beyond sixfold coordinated Si in SiO_2 glass at ultrahigh pressures," Proc. Natl. Acad. Sci. U. S. A. **114**, 10041–10046 (2017).
[68]S. Speziale, C.-S. Zha, T. S. Duffy, R. J. Hemley, and H.-k. Mao, "Quasi-hydrostatic compression of magnesium oxide to 52 GPa: Implications for the pressure-volume-temperature equation of state," J. Geophys. Res. **106**, 515–528 (2001).
[69]Y. Akahama and H. Kawamura, "Pressure calibration of diamond anvil Raman gauge to 410 GPa," J. Phys.: Conf. Ser. **215**, 012195 (2010).
[70]C. Ji, B. Li, W. Yang, and H. Mao, "Crystallographic studies of ultra-dense solid hydrogen," Chin. J. High Pressure Phys. **34**(2), 20101 (2020).
[71]M. Eriksson, J. F. van der Veen, and C. Quitmann, "Diffraction-limited storage rings: A window to the science of tomorrow," J. Synchrotron Radiat. **21**, 837–842 (2014).